ABCM 40 anos
Associação Brasileira de Engenharia e Ciências Mecânicas
CONEM 2016
CONGRESSO NACIONAL DE ENGENHARIA MECÂNICA
21 - 25 AGOSTO DE 2016
FORTALEZA - CEARÁ

Direct simulation of fluid lubricated contacts down to the surface roughness scale (CODIGO: CON-2016-1311)

Author 1[1]
Author 2[1]
Author 3[1]
Author 4[2]
Author 5[1]

[1] INSTITUTION 1
[2] INSTITUTION 2

Abstract:
Mechanical losses in a car engine are due mostly to fluid bearings. Fluid bearings in car engines are present in the ring/liner contact, connecting rod, crankshaft bearings, valves, valve seats, camshaft contacts and seals in general, accounting for 10% of the fuel consumption, more than half of it being due to the piston assembly (Holmberg et al.*, 2012). Microengineering techniques such as honing, ion beam texturing, etching and laser surface texturing among others (Etsion, 2005) have made viable to shape the surfaces of these devices down to the scale of the surface roughness. These patterned microstructures often come in the form of pockets, dimples and grooves, aiming to improve the load capacity, wear rate and reduce friction.*
Several experimental and theoretical studies have established the possibility of improving the performance of fluid bearings by controlling the topography of the surfaces, however, the fundamentals of why this takes place are not fully understood. Furthermore, determining the best surface in terms of friction and wear for each working condition by means of experimental procedures is a expensive process. What's more, accurate measurements of point-wise quantities like film thickness or pressure are extremely difficult. A practical approach is the mathematical modeling and numerical simulation of lubricated contacts.
In this paper the lubrication problem taking into account cavitation effects and the bearing dynamics has been solved for realistic operational conditions. A mass-conserving model is used to treat cavitation. Textures have been set on the moving surface of the lubricated pair. Most researchers have tackled this problem considering non-moving surfaces and neglecting the bearing dynamics to reduce the computational burden. Our approach is more encompassing and complex than previous ones, as each simulation is intrinsically transient. Parametric studies of micro-textured surfaces and simulations with surfaces of known measured topography corresponding to various surface finishings such as honings were performed with a discretization finer than the measurements. This led to a better understanding of the mechanics of friction reduction with micropatterned and rough surfaces.
To be able to solve these large problems in acceptable time, numerical and computational techniques must be used. These studies were made possible by an efficient and robust parallel multigrid algorithm to solve the hydrodynamics coupled with the bearing dynamics. The present work summarizes some of the contributions of Hugo Checo's PhD thesis (Checo, 2016) to the simulation and assessment of realistic surfaces in fluid bearings.

Keywords: *honed surfaces, numerical methods, cavitation, fluid bearing, numerical simulation.*

1. INTRODUCTION

Fluid-dynamic bearings are present in many key high-load, high-speed precision applications where other mechanisms like ball bearings would not perform as well due to noise and vibrations, or because is it even impossible to apply another solution. In car engines they are present in the piston assembly, crankshaft bearings, valves, valve seats, camshaft contacts and seals in general. The piston assembly accounts for 50% of the engine friction losses, which is approximately 10% of the total fuel consumption. Half of that takes place in the piston ring/liner contact (Holmberg *et al.*, 2012), thus being one of the major contributors to the mechanical power losses. Thus, it is important to understand the key factors influencing film formation and friction in fluid film bearings.

All the mentioned engine components work under severe loading conditions. A complete separation of both bearing surfaces (*hydrodynamic* lubrication regime) is not assured, and partial solid-solid lubrication (*mixed* lubrication regime) or mainly solid-solid contact (*boundary* lubrication regime) takes place. Under these conditions the real topography of the surfaces is a determining factor in the bearing performance.

Surface texturing has attracted much attention in the last years as a new mean to improve the tribological performance of lubricated contacts, especially since surface microengineering techniques have become available. Honing, machining, ion beam texturing, etching and laser surface texturing are some of the techniques used (Etsion, 2005). Micropatterned surfaces usually consist of pockets (dimples) with dimensions in the order of tens or hundreds of microns, honed grooves are on the tens of microns and the surface roughness level is even smaller, in the order of the micron or even lower. With a domain in the centimeters (size of the ring pack, journal bearing, seal, etc), this enforces the use of very fine meshes which is traduced in a greater computational cost. In this work a efficient numerical method to solve thin film (lubrication) problems down to the roughness scale is presented. As an application, these methods will help with the assessment of rough and micro-patterned surfaces in the performance of fluid lubricated bearings.

This paper is organized as follows: a general model for fluid lubricated bearings is presented Section 2. Section 3. briefly presents the numerical methods employed to solve the previous model. Results of numerical simulations with micro-textured and rough surfaces are given in Section 4. Finally, conclusions are drawn in Section 5.

2. MODELING OF LUBRICATED CONTACTS

The arrangement of Figure 1(a) shows a pad sliding over a textured surface (the runner) with velocity $-u(t)$. This configuration is more typical of a piston-ring/liner contact, as the strip in red shows in Figure 1(b), however, the mathematical formulation of the problem remains general enough to represent other lubricated contacts (e.g., journal-bearing-like devices), as explained in Checo (2016). The domain is a strip $\Omega = (x_\ell, x_r) \times (0, w)$. Notice that the domain is two-dimensional, in the directions x_1 and x_2: Figure 1(a) shows just a section along x_1. The geometry is determined by the functions h_U and h_L describing the upper (fixed) surface and lower (moving) surfaces respectively, and $Z(t)$, which parametrizes the pad movement.

The pad dynamics is governed by Newton's Second Law. The forces $W(t)$ acting on it are the applied ones (force of the gases of the combustion chamber, elastic forces) and the reactive forces. The latter ones come from the interaction between the pad and the lubricating oil (the hydrodynamic forces) and between the pad and the sliding surface (contact forces), here named $W^h(t)$ and $W^c(t)$ respectively. $W^c(t)$, usually given by the Greenwood-Tripp model (Greenwood and Williamson, 1966), is a function of the separation $Z(t)$ between the surfaces. To be able to compute W^h, the hydrodynamics must be solved first. Due to the geometry of the contacts and the high velocities involved *cavitation* takes place. It has been shown by Ausas et al (Ausas *et al.*, 2009b) that a mass-conserving model is of foremost importance, which is confirmed by several authors, among them Zhang and Meng (2012) who performed a careful comparison with experiments. Here we employ the Elrod-Adams model (Elrod and Adams, 1974), which includes into the Reynolds equation conservative boundary conditions for cavitation.

The complete non-dimensional mathematical problem (details of the non-dimensionalization can be seen in Checo *et al.* (2014)) to be solved reads:

"Find trajectory $Z(t)$, and fields $p(t)$, $\theta(t)$, defined on $\Omega \times [0,T] = \{(x_\ell, x_r) \times (0,w)\} \times [0,T]$ and periodic in x_2, satisfying

$$\begin{cases} Z(0) = Z_0, \qquad Z'(0) = V_0, \\ \theta(x_\ell, x_2, t) = d_{\text{lub}}/h(x_\ell, x_2, t) \qquad \forall x_2 \in (0,w)\,,\ \forall t \\ \theta(x_r, x_2, t) = d_{\text{lub}}/h(x_r, x_2, t) \qquad \forall x_2 \in (0,w)\,,\ \forall t \\ p > 0 \quad \Rightarrow \quad \theta = 1 \\ \theta < 1 \quad \Rightarrow \quad p = 0 \\ 0 \le \theta \le 1 \end{cases}, \tag{1}$$

and

$$m\frac{d^2 Z}{dt^2} = W(t) + W^h(t) + W^c(t)\,, \tag{2}$$

$$\nabla \cdot \left(h^3 \nabla p\right) = u(t)\,\frac{\partial\, h\theta}{\partial x_1} + 2\frac{\partial\, h\theta}{\partial t}\,, \tag{3}$$

where

$$h(x_1, x_2, t) = \begin{cases} h_L(x_1 - u\,t, x_2) + h_U(x_1, x_2) + Z(t) & \text{if } a \le x_1 \le b \\ h_L(x_1 - u\,t, x_2) + e & \text{otherwise} \end{cases}, \tag{4}$$

$$W^h(t) = \frac{1}{w}\int_a^b \int_0^w p(x_1, x_2, t)\, dx_1\, dx_2\,, \tag{5}$$

$$W^c(t) = \frac{1}{w}\int_0^w \int_a^b p_{\text{con}}(x_1, x_2, t)\, dx_1\, dx_2, \tag{6}$$

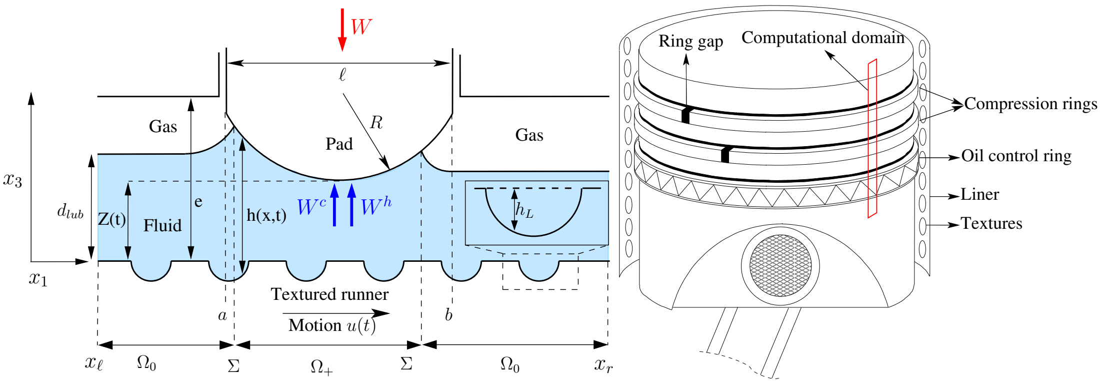

(a) (b)

Figura 1: Figure (a) depicts a section of the domain along the pad (bearing surface in general, e.g.: piston ring) direction of motion, along with the forces acting on it. Figure (b) shows a scheme of a ring pack placed in the piston. The computational domain is bounded by a red rectangle.

functions $h_L(x_1, x_2, t)$, $h_{U_i}(x_1, x_2)$, $W(t)$ and $u(t)$ are known explicitly, d_{lub} and e are positive constants, m is the pad's mass and the contact pressure p_{con} is given by the Greenwood-Tripp model."

Textures are set on the moving surface of the lubricated pair. Moving textures are more challenging from the numerical point of view since the problem becomes intrinsically transient. Then, the dynamics of the pad must be solved coupled with the hydrodynamics and the other forces involved.

The tribological quantities computed are the *clearance*

$$C(t) = \min_{(x_1,x_2)\in\Omega} h(x_1, x_2, t) \ , \tag{7}$$

and the hydrodynamic *friction force*

$$F(t) = -\frac{1}{w}\int_a^b \int_0^w \left(\frac{u\, g(\theta)}{h} + 3h\frac{\partial p}{\partial x_1} - 6p\frac{\partial h_L}{\partial x_1} \right) dx_1\, dx_2 \ , \tag{8}$$

here also in non-dimensional form. Function g is defined by

$$g(\theta) = \begin{cases} \theta & \text{if } \theta > \theta_s \\ 0 & \text{otherwise.} \end{cases} \tag{9}$$

The parameter θ_s is a threshold for the onset of friction, which can be interpreted as the minimum oil fraction for shear forces to be transmitted from one surface to the other. Here is taken as θ_s=0.95 for all cases. The instantaneous friction coefficient for the pad then results from

$$f(t) = \frac{-F(t)}{W(t)} \ , \tag{10}$$

while the load carrying capacity $L(t)$ is defined by $L(t) = W^h(t)$. When periodicity was established in the simulations the quantities computed were the *average friction coefficient*

$$\overline{f} = \frac{1}{\lambda/V_1}\int_T^{T+\lambda/V_1} f(t)\, dt \tag{11}$$

which characterizes the power lost to friction, and the *minimum clearance*

$$C_{\min} = \min_{T\le t\le T+\lambda/V_1} C(t) \tag{12}$$

which can be used to characterize wear.

3. NUMERICAL METHODS

The pad dynamics (equation 2) are solved iteratively through a Newmark scheme, coupled with the hydrodynamics. The conservative finite volume method described in Ausas *et al.* (2009a) is used to discretize the Elrod-Adams equation (eq. 3). An efficient numerical solution for the Elrod-Adams model is by no means trivial, as the classical Newton-Raphson method is not suitable for this problem. The best approach so far is to solve it with a Jacobi or Gauss-Seidel type algorithm, as done by Ausas *et al.* (2009a). However, it becomes computationally expensive for large problems, due to the elliptic problem being solved for the pressure. Multigrid methods arise like a natural choice to accelerate results, yet its implementation for the Elrod-Adams model is not straightforward. A shifting of the cavitation boundary takes place in the coarser meshes, which was already recognized by Venner and Lubrecht (2000). In Checo (2016) an efficient and robust multigrid implementation is presented, which preserves in the coarser meshes the position of the cavitation boundary computed in the finest mesh. This algorithm was implemented in a parallel shared-memory framework.

4. MICROPATTERNED AND MEASURED SURFACE SIMULATIONS

4.1 Friction reduction and lift generation with moving pocketed surfaces

We have studied the consequences of texturing the runner surface on the tribological performance of a generic pad/runner contact (observations are then applicable to other devices, such as thrust bearings and lip seals) with fixed loads and fixed runner velocity, that corresponds to hydrodynamic lubrication conditions (that is, no contact forces were present).

The study was carried on through 720 two dimensional mesh-converged runs, each of which involved a transient dynamically-coupled calculation. The pockets on the surface are semi-ellipsoids as the ones shown in figure 2, set in a square lattice of period λ. Parameters l, λ and d varied in the ranges 10-300, 50-600 and 2-30 micrometers. The pad length was set to b-a=1 mm.

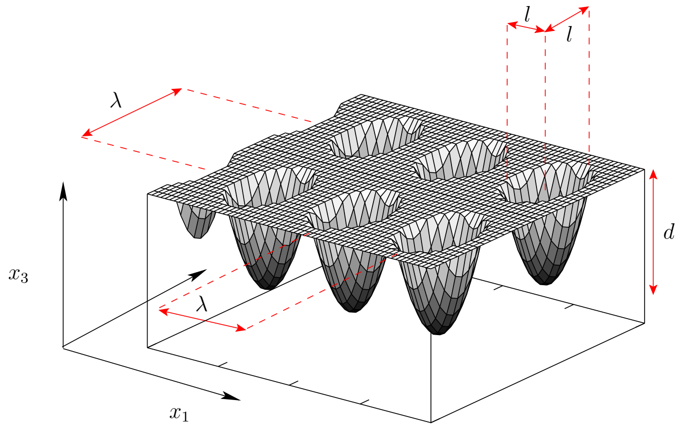

Figura 2: Dimples on the runner surface. λ, l and d are the texture's period, radius and depth.

The main observations were that the pad profile, here controlled by variable R as seen in figure 1(a), determines whether texturing the surface is beneficial or not, and that the flatter the contact, the greater reduction in friction that can be obtained from texturing the moving surface. This is the central result of figure 3. Each dot represents the results of one simulation. The vertical axes are the average friction coefficient $\overline{f}$ (load was kept constant for all cases, so the comparison is fair) and the minimum clearance C_{min}. Despite the better performance of large R bearings with textured surfaces compared to the same results with untextured surfaces (red line), highly convergent/divergent pads show better performance than their flat, textured counterparts. This is interesting if it is realized that during the bearing life it undergoes wear, and thus becomes flatter, making textured surfaces interesting in the long run. These results are consistent with several experimental studies (Mishra and Polycarpou (2011); Ramesh *et al.* (2013); Yuan *et al.* (2011); Wang *et al.* (2006); Bifeng *et al.* (2012); Cho and Park (2011)). On the other hand, opposite results have been reported in a few cases (Pettersson and Jacobson (2007); Kovalchenko *et al.* (2005)).

The best performance (lowermost points in fig.3(a), uppermost in 3(b)) is achieved with texture lengths comparable with the size of the contact, and depths similar to the pad-to-slider clearance. Details of these results can be found in Checo *et al.* (2014, 2015).

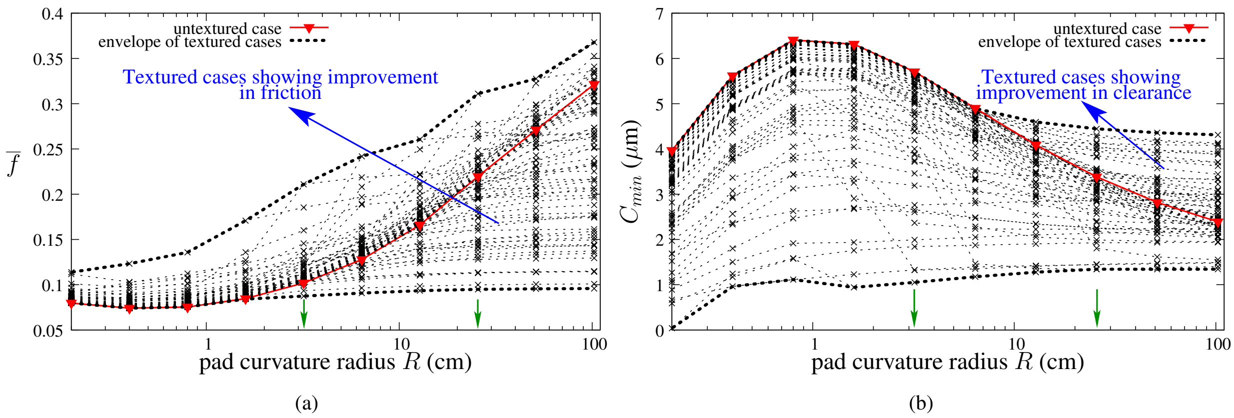

Figura 3: (a) Friction coefficient and (b) minimum clearance for all the 720 simulations of pocketed surfaces.

These results were extended for other operational conditions in a broader study Checo *et al.* (2015), and checked analyzing 10.000 one-dimensional simulations with several pad masses and loads, and sinusoidal textures

$$h_t(x) = d\,\frac{\cos(2\,\pi\,x/\lambda)\,-\,1}{2}\,, \tag{13}$$

on the moving surface. This was done at two R values of interest of figure 3, shown there with small green arrows. The maps of figure 4 show the percentage decrease (increase) in friction (clearance). The general trends and underlying physical mechanisms of friction reduction of the two-dimensional study were confirmed.

The study was also useful to identify more interesting physical phenomena, as the seen in the lower right corner of figures 4(a) and 4(b) (inside the red ellipse). This discontinuity, whose origin explained in (Checo *et al.*, 2015), suggests caution against carelessly choosing surface textures.

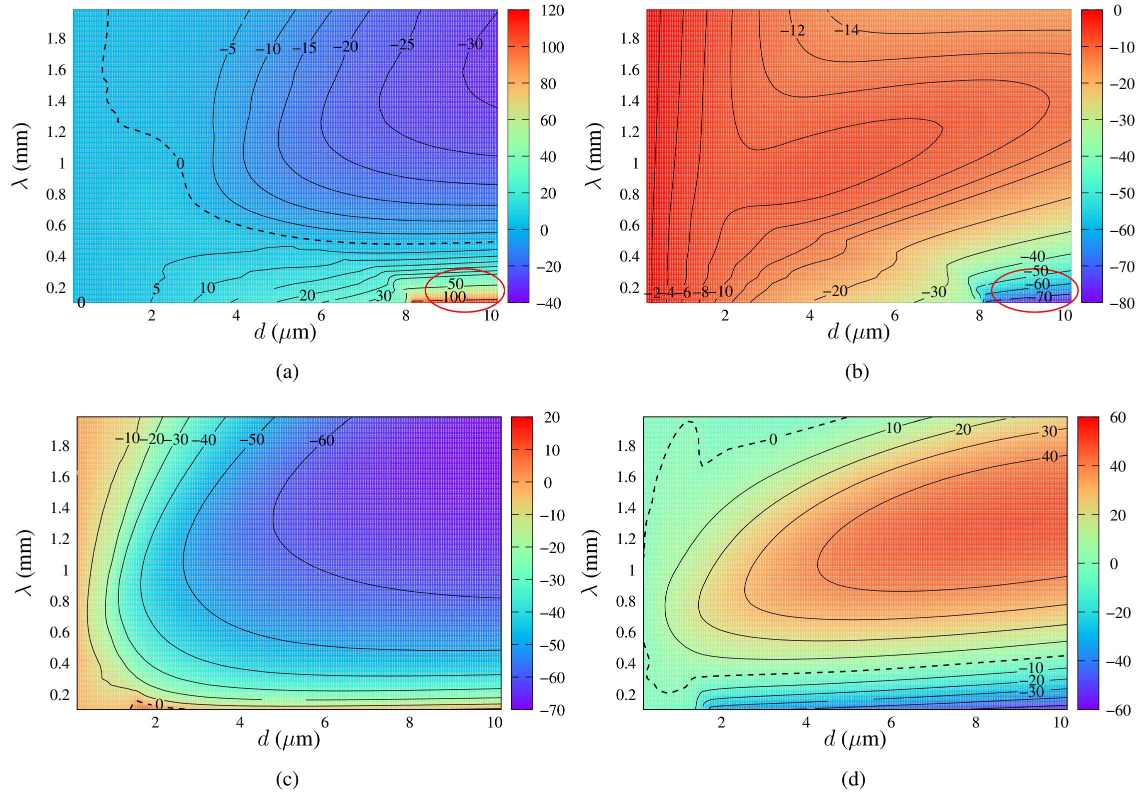

Figura 4: Percentage reduction in (a) friction and (b) clearance with respect to the untextured runner, as functions of the texture parameters d and λ for a ring with R=3.2. The colorbars (as the isolines) indicate these percentages. Parts (c) and (d) of the Figure show analogous plots for R=25.6.

4.2 Measured surface simulations

Surface roughness is usually treated in lubrication problems by means of stochastic models (Tzeng and E. (1967); Christensen (1969)), averaged models (Patir and Cheng Patir and Cheng (1978, 1979)) or homogenization methods (Bayada *et al.* (1988, 1989); Jai (1995); Buscaglia *et al.* (2002); Buscaglia and Jai (2004)). In this work, the uncertainties associated with such methods are avoided using the measured topography of the surface. Space and time converged simulations were performed, and the influence of the surface's topography in friction, load carrying capacity (hydrodynamic lift) were analyzed. To the extent of our knowledge, it was the first time that direct simulations both in space and time where carried on rough surfaces. This means that both the spatial and time discretization were small enough to capture all the surface features plus the bearing dynamics.

Figure 5 illustrates a specific topography, corresponding to a honed cylinder liner of a car engine. Figure 5(b) shows it in perspective, along with the width of the pad employed in the simulations. A proper way to characterize a honed surface is by means of its Abbott-Firestone parameters Abbott and Firestone (1933). Its related roughness parameters R_k (plateau height), R_{pk} (reduced peak height), R_{vk} (reduced valley height), M_{r1} (percentage of R_{pk} peaks) and M_{r2} (1-M_{r2} can be understood as the percentage of R_{vk} valleys) are shown in Table 1, along with the more conventional parameters S_a (roughness average), S_q (root mean square roughness), S_{sk} (skewness) and S_{ku} (kurtosis).

Each measurement point corresponds to a 2μm$\times$2μm cell. This gives for the measured surface a total of 810.000 measurement points. Computational domains are usually larger than the sample size, so the total number of cells required to solve the problem can reach several million. Convergence studies suggest a mesh spacing of one fourth of the measurement with a Courant number of 1.0 (Checo *et al.*, 2016). This further increases the computational burden.

Deterministic simulations of actual liner surfaces face a wide variety of challenges. Ring, piston and fluid dynamics, contact forces among others must be modeled. Once this has been dealt with, there remains the difficulties associated with the numerics. Supposing a domain large enough to hold all three rings of a pack, of 15 mm in the movement direction and 1.8 mm in the radial direction (the complete width of the measured surface of figure 5), a structured mesh large enough to capture the level of detail of the surface would have approximately *32 million finite volumes*. If a Courant number

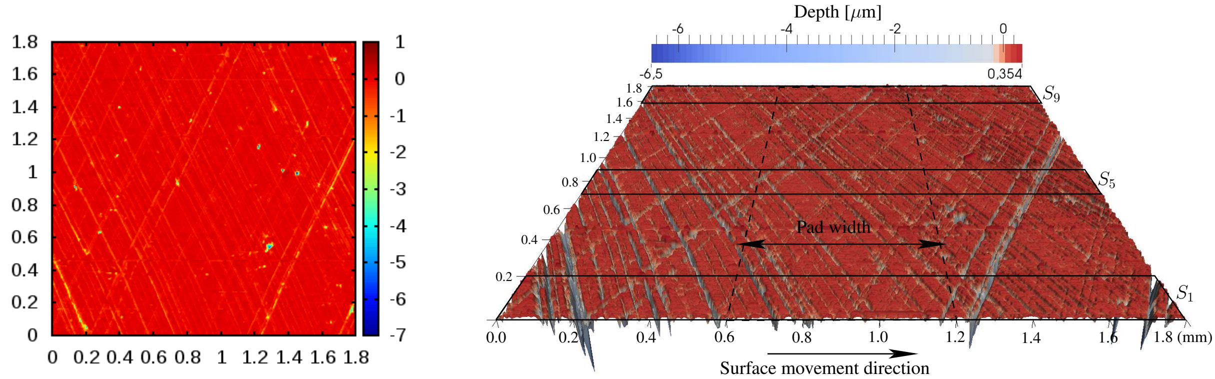

(a) (b)

Figura 5: (a) A 1.8×1.8 mm sample of a honed engine liner; (b) A perspective of the sample, with the pad width b-a for comparison and the size of the stripes S_1 to S_9 in which it was divided.

Parameter	Value
S_a	0.15 μm
S_q	0.25 μm
S_{sk}	-6.56
S_{ku}	81.8
R_{pk}	0.18 μm
R_k	0.2 μm
R_{vk}	6.47 μm
M_{r1}	6.6%
M_{r2}	75.9%

Tabela 1: Surface-finish parameters for the surface of Figure 5.

of 1 is to be kept with a constant time step Δt, more than *a million* iterations in time will be necessary to simulate just one engine cycle. This, in a single desktop machine will take **months** to compute. However, some pre-processing and approximations can be done to decrease the computational time.

First, it is not necessary to simulate over the whole sample. If the sample is divided into strips of a certain size in the movement direction, the quantities of interest computed on them are representative of the results for the whole sample, as seen in Table 2. Here, a reasonable size was 200μm (strips S_1 to $S - 9$ of Figure 5), which led to errors smaller than 2.1%. This reduced domain size decreases the workload considerably.

Strip	$\overline{L(t)}$ (N)	$\overline{F(t)}$ (10^{-3}N)
1	1.905	21.10
2	2.138	21.35
3	2.009	21.50
4	2.089	21.26
5	2.073	21.49
6	2.148	21.59
7	2.167	21.73
8	2.226	21.47
9	2.178	21.43
Sum	18.993	192.92
Whole surface	18.6	192.53
Difference	2.1 %	0.2%

Tabela 2: Average hydrodynamic lift $\overline{L(t)}$ and friction force $\overline{F(t)}$ for the nine contiguous strips of width 0.2 mm in which the surface of figure 5 is subdivided, and for the whole surface. Z=0.5 μm stands for all nine simulations.

It is clear that the large scale of the bearing (its main shape) is a determining factor in its efficiency. If Z is large enough compared with the surface's roughness, then h_L is a small perturbation on h, and it is expected that the problem solution will be governed by the length scale of the bearing. Table 3 shows the difference between the results of the average friction force and hydrodynamic lift extracted from the simulations taking into account surface roughness, and simulations with a untextured surface ($h_L \equiv 0$):

$$e^F_{untext} = \left| \frac{F_{untext} - F}{F} \right| . \tag{14}$$

$$e^L_{untext} = \left| \frac{L_{untext} - L}{L} \right| . \tag{15}$$

For Z=0.5 μm, the error in friction is above 10% and as high as 24%. However, for $Z \geq$2.0 μm the errors rapidly decrease and are lower or equal to 6%. In hydrodynamic lift the errors are still considerable for Z=4.0 μm, larger than 8%. A noticeable trend is that errors for $R = 0.8$ cm are significantly smaller. This is due to the fact that for a more pronounced wedge the average h is larger. The later results are remarkable due to the low errors attained and to the fact that a computationally inexpensive problem (one-dimensional) is being solved instead of a complex measured-surface simulation. Nevertheless, in highly loaded applications such as the piston-ring/liner contact, clearances are in the order of the tenth of the micrometer, and thus the surface roughness must be considered.

	e^F_{untext} (%)				e^L_{untext} (%)			
R (cm)	Z =0.5 (μm)	1.0	2.0	4.0	0.5	1.0	2.0	4.0
0.8	-11.2	-5.0	-2.3	-1.2	-8.4	-3.5	-1.7	-0.9
12.8	-23.9	-13.1	-6.0	0.2	-20.0	-11.9	-9.0	-8.6

Tabela 3: Percentage errors e^F_{untext} and e^L_{untext} committed by neglecting the surface roughness.

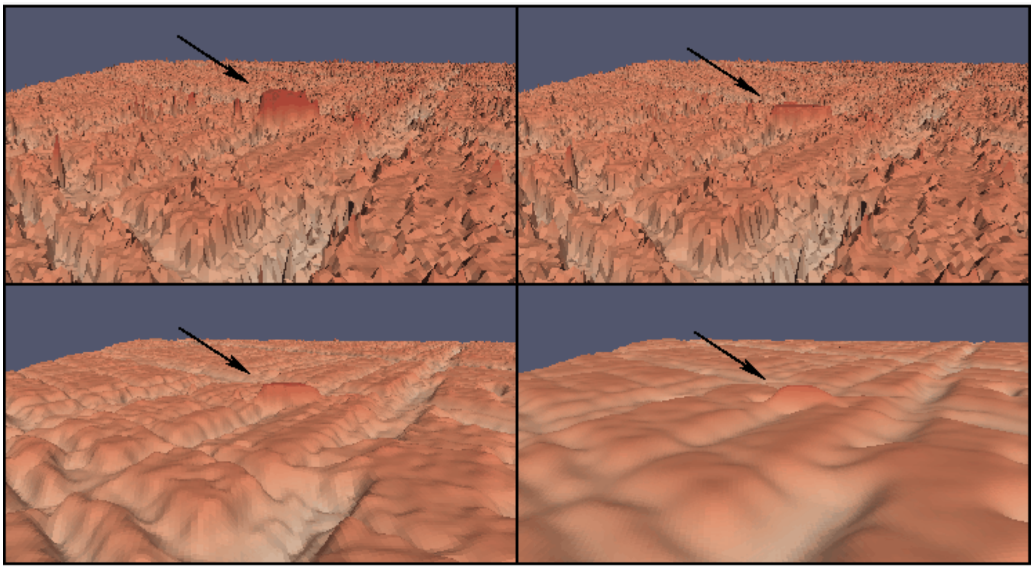

Figura 6: Successive stages in pre-processing: (top-left) unprocessed; (top-right) the highest peaks have been removed; (below-left) surface smoothed 3 times, and (below-right) surface smoothed 20 times. In all figures the most prominent asperity is pinpointed by a black arrow.

Some pre-processing can be done to the measured surface to alleviate the computational burden. A fraction of the surface is shown in top left Figure 6. The honed grooves and asperities can be observed. Among the latter, the one indicated by the black arrow protrudes more than the others. This asperity is most likely to be eliminated by wear during the running-in of the engine. Leaving the surface as it is will lead to results in the quantities of interest (friction, clearance) that might not be representative of the engine performance in the long run. Besides, from the numerical point of view it will generate some violent behavior in the simulations which can be really hard to capture. To deal with this, peaks in surface were removed. Figure 6 shows (top, left) the original surface and the same after peak-removal (top, right). It can be seen that the surface characteristics are maintained, aside from the atypical spikes.

Another measured-surface data pre-processing technique with the only objective to render simulations computationally more amenable is surface smoothing. Each measured point is now taken as the average of the points around it. This is done in several smoothing sweeps across the measured surface. Both bottom images in Figure 6 show the outcome for 3 (bottom, left) and 20 (bottom, right) sweeps. To compare the differences in the results for each of the four surfaces of Figure 6, simulations are run in a section of the domain, corresponding to the Strip S_5 of Figure 5. Table 4 shows the computational time in a 4-cored Intel i7-4810MQ processor for each run. As can be seen, removing peaks reduces the computational time in only 1.4%, however the smoothing procedure decreases it greatly. Solving the problem with the 20-sweep surface takes just one third of the time than solving it on the original surface.

Surface	Time (s)	Decrease in time (%)	Error in $Z(t)$	Error in $\overline{F(t)}$
As received	1010.5	–		
Only peaks removed	996.4	1.4	2.5%	4.1%
3 averaging sweeps	601.2	40.5	4.1%	6.5%
20 averaging sweeps	326.7	67.7	5.1%	7.7%

Tabela 4: Computational time savings with surface data pre-processing.

But how about the errors committed by modifying the original surface?. Figure 7 shows the results. For the surface with peaks removed and three smoothing sweeps the ring displacement $Z(t)$ did not change more than 5%, while the difference in the average friction force $\overline{F(t)}$ over the last passage of the texture under the ring is less than 7%. Friction, as expected, tends to decrease with this surface pre-processing, specially those spikes seen in Figure 7(c) at $t = 2 \times 10^{-4}$ and $t = 4.5 \times 10^{-4}$, caused by the higher summits of the untreated surface.

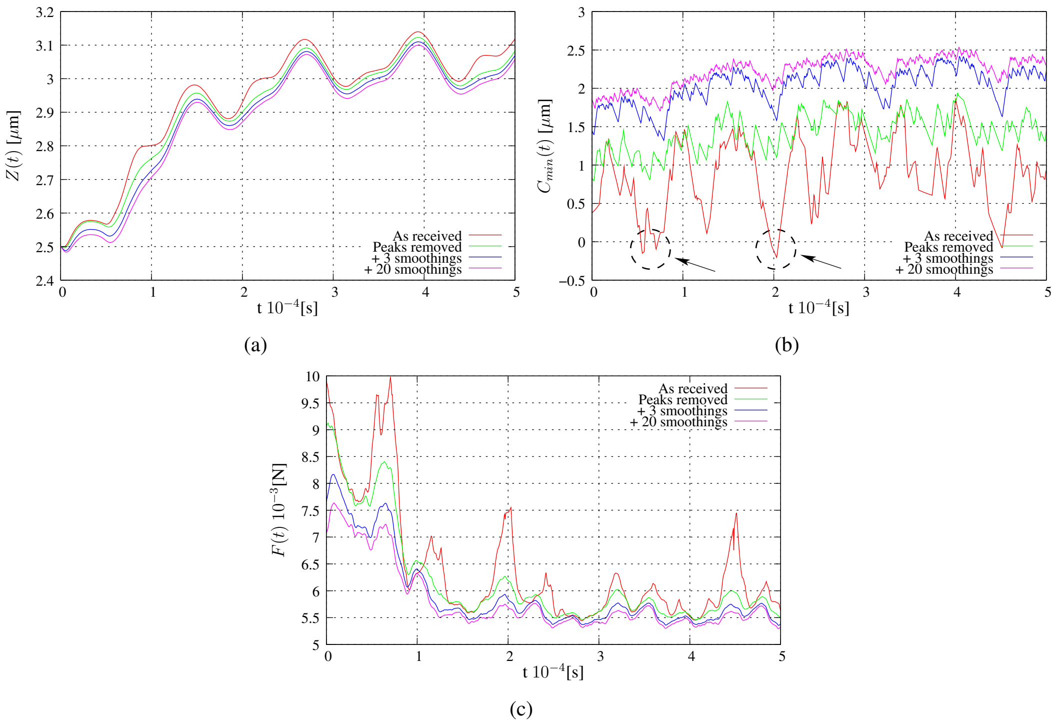

Figura 7: (a) Ring position, (b) minimum clearance and (c) friction force for Strip S_5 of figure 5(b) without modifications, with peaks removed, and with peaks removed and some smoothing.

Another problem related with high peaks is surface penetration. A closer look at Figure 7(b) shows some negative C_{min} values, which are indicated by the black arrows. These negative values take place due to: a) a high asperity moving towards the ring already at a low $Z(t)$ position; b) insufficient hydrodynamic and contact force support to hold the load imposed on the ring, and c) a large time step Δt, not able to capture the rapid dynamics of the ring. For the load used in this tests, a) is the most probable cause of penetration as C_{min} is not only positive, but also much higher after peak-removal. None of the other three cases shown in Figure 7(b) displayed this problem.

All these strategies help to decrease computational times, aiming to solve the piston-ring/liner contact. In Checo

(2016) several simulations of two complete engine cycles in realistic conditions and with measured surfaces a presented, performed with a single desktop computer in less than 24 hours.

Surface	Error in $Z(t)$	Error in $\overline{F(t)}$
Only peaks removed	2.5%	4.1%
3 averaging sweeps	4.1%	6.5%
20 averaging sweeps	5.1%	7.7%

Tabela 5: Percentage errors of the modified surfaces with peaks removed and with peaks removed and smoothing.

5. CONCLUSIONS

In this work we have summarized the modeling, numerical treatment, numerical studies of micro-textured and rough moving surfaces in fluid lubricated contacts. The problem of a pad sliding over a surface is solved considering its dynamics and taking into account cavitation in the hydrodynamics. The pad dynamics are governed by the hydrodynamic forces and the solid-solid forces arising from the contact of both the pad and the slider.

The Elrod-Adams model was solved with the Finite Volume Method, and the pad dynamics are solved coupled with the hydrodynamic using a Newmark marching scheme, built in the overall iterative process.

A systematic study of moving micro-textured surfaces with a mass-conservative cavitation model was performed, so that the mechanisms responsible for friction reduction in the hydrodynamic lubrication regime can be understood. This study was made feasible in great manner due to the multigrid implementation and a shared memory parallelization.

Another major outcome was the simulation of lubricated contacts considering the measured topography of honed cylinder liners of car engines. It was seen that for low to moderately loaded devices, where clearances are much higher than the surface roughness, the error committed by neglecting surface roughness is low. Nevertheless, for devices that normally operate in mixed lubrication regimes it is necessary to take it into account. The overwhelming computational requirements are relieved by means of some pre-processing on the surfaces of measured topography and some approximations, which lead to cheaper solutions of low error.

6. ACKNOWLEDGEMENTS

The authors thank the financial support of this work provided by CAPES (grant PROEX-8434433/D), FAPESP (grants 2011/24147-5 and 2014/19249-1) and CNPq (grant 447904/2014-0).

7. REFERÊNCIAS

Abbott, E. and Firestone, F., 1933. “Specifying Surface Quality - A Method Based on Accurate Measurements and Comparison.” *Journal of Mechanical Engineering*, Vol. 55, pp. 569–572.

Ausas, R., Jai, M. and Buscaglia, G., 2009a. “A Mass-Conserving Algorithm for Dynamical Lubrication Problems With Cavitation”. *ASME Journal of Tribology*, Vol. 131, p. 031702 (7 pages).

Ausas, R., Ragot, P., Leiva, J., Jai, M. Bayada, G. and Buscaglia, G., 2009b. “The impact of the Cavitation model in the Analysis of Micro-Textured Lubricated Journal bearings.” *ASME Journal of Tribology*, Vol. 129, pp. 868–875.

Bayada, G., Chambat, M. and Faure, J., 1988. “Some effects of the boundary roughness in a thin film. Boundary control and boundary variations.” *Lecture Notes in Compu Sci.*, Vol. 100, pp. 96–115.

Bayada, G., Chambat, M. and Faure, J., 1989. “A Double Scale Analysis Approach of the Reynolds Roughness. Comments and Application to the Journal Bearing.” *ASME Journal of Tribology*, Vol. 111, pp. 323–330.

Bifeng, Y., Li, X., Fu, Y. and Yun, W., 2012. “Effect of laser textured dimples on the lubrication performance of cylinder liner in diesel engine”. *Lubrication Science*, Vol. 24, pp. 293–312.

Buscaglia, G., Ciuperca, I. and Jai, M., 2002. “Homogenization of the transient Reynolds equation ”. *Asymptotic Analysis*, Vol. 32, pp. 131–152.

Buscaglia, G. and Jai, M., 2004. “Homogenization of the Generalized Reynolds Equation for Ultra-Thin Gas Films and Its Resolution by FEM ”. *ASME Journal of Tribology*, Vol. 126, p. 547.

Checo, H., Ausas, R., Jai, M., Cadalen, J.P., Choukroun, F. and Buscaglia, G., 2014. “Moving textures: Simulation of a ring sliding on a textured liner”. *Tribology International*, Vol. 72, pp. 131–142.

Checo, H., Jaramillo, A., Jai, M. and Buscaglia, G., 2015. “Texture-induced cavitation bubbles and friction reduction in the Elrod-Adams model”. *Proc IMechE Part J: J Engineering Tribology*, Vol. 229(4), pp. 478–492.

Checo, H., Jaramillo, A., Jai, M. and Buscaglia, G., 2016. “The lubrication approximation of the friction force for the simulation of measured surfaces.” *Tribology International*, Vol. 97, pp. 390–399.

Checo, H., 2016. *Models and methods for the direct simulation of rough and micropatterned surfaces*. Ph.D. thesis, Instituto de Ciências Matemáticas e de Computação, Universidade de São Paulo.

Cho, M. and Park, S., 2011. "Micro CNC surface texturing on polyoxymethylene (POM) and its tribological performance in lubricated sliding". *Tribology International*, , No. 44, pp. 859–867.

Christensen, H., 1969. "Stochastic Models of Hydrodynamic Lubrication of Rough Surfaces". *Proc, Int. Mech. Eng*, Vol. 55, p. 1013.

Elrod, H.G. and Adams, M., 1974. "A computer program for cavitation. Technical report 190." *1st LEEDS LYON Symposium on Cavitation and Related Phenomena in Lubrication, I.M.E.*, Vol. 103, p. 354.

Etsion, I., 2005. "State of the art in laser surface texturing". *J, Tribol.: Trans. ASME*, Vol. 127, pp. 248–253.

Greenwood, J. and Williamson, J., 1966. "Contact of Nominally Flat Surfaces". *Proceedings of the Royal Society of London. Series A, Mathematical and Physical Sciences*, Vol. 295, pp. 300–319.

Holmberg, K., Andersson, P. and Erdemir, A., 2012. "Global energy consumption due to friction in passenger cars". *Tribology International*, Vol. 47, pp. 221–234.

Jai, M., 1995. "Homogenization and two-scale convergence of the compressible Reynolds lubrication equation modeling the flying characteristics of a rough magnetic head over a rough rigid-disk surface." *Math. Modeling and Numer. Anal.*, Vol. 29, pp. 199–233.

Kovalchenko, A., Ajayi, O., Erdemir, A., Fenske, G. and Etsion, I., 2005. "The effect of laser surface texturing on transitions in lubrication regimes during unidirectional sliding contacts". *Tribology International*, Vol. 38, pp. 219–225.

Mishra, S.P. and Polycarpou, A.A., 2011. "Tribological studies of unpolished laser surface textures under starved lubrication conditions for use in air-conditioning and refrigeration compressors". *Tribology International*, Vol. 44, pp. 1890–1901.

Patir, N. and Cheng, H., 1978. "An Average Flow Model for Determining Effects of Three-Dimensional Roughness on Partial Hydrodynamic Lubrication". *Transactions of the ASME*, Vol. 100, pp. 12–17.

Patir, N. and Cheng, H., 1979. "Application of Average Flow Model to Lubrication Between Rough Sliding Surfaces". *Transactions of the ASME*, Vol. 101, pp. 220–229.

Pettersson, U. and Jacobson, S., 2007. "Textured surfaces for improved lubrication at high pressure and low sliding speed of roller/piston in hydraulic motors". *Tribology International*, Vol. 40, pp. 355–359.

Ramesh, A., Akram, W., Mishra, S.P., Cannon, A.H., Polycarpou, A.A. and King, W.P., 2013. "Friction characteristics of microtextured surfaces under mixed and hydrodynamic lubrication". *Tribology International*, Vol. 57, pp. 170–176.

Tzeng, S. and E., S., 1967. "Surface Roughness Effect on Slider Bearing Lubrication". *ASLE Transactions*, Vol. 10, pp. 334–338.

Venner, C. and Lubrecht, A., 2000. *Multilevel methods in lubrication*. Elsevier.

Wang, X., Adachi, K., Otsuka, K. and Kato, K., 2006. "Optimization of the surface texture for silicon carbide sliding in water". *Applied Surface Science*, Vol. 253, pp. 1282–1286.

Yuan, S., Huang, W. and Wang, X., 2011. "Orientation effects of micro-grooves on sliding surfaces". *Tribology International*, Vol. 44, pp. 1047–1054.

Zhang, J. and Meng, Y., 2012. "Direct observation of cavitation phenomenon and hydrodynamic lubrication analysis of textured surfaces". *Tribology Letters*, Vol. 46, pp. 147–158.